

Experimental Evidence of Interatomic Coulombic Decay from the Auger Final States in Argon Dimers

Y. Morishita,¹ X.-J. Liu,² N. Saito,^{1,*} T. Lischke,² M. Kato,¹ G. Prümper,² M. Oura,³ H. Yamaoka,³ Y. Tamenori,⁴
I. H. Suzuki,¹ and K. Ueda^{2,†}

¹National Institute of Advanced Industrial Science and Technology (AIST), NMIJ, Tsukuba 305-8568, Japan

²Institute of Multidisciplinary Research for Advanced Materials, Tohoku University, Sendai 980-8577, Japan

³RIKEN, Harima Institute, Sayo, Hyogo 679-5148, Japan

⁴Japan Synchrotron Radiation Research Institute, Sayo, Hyogo 679-5198, Japan

(Received 17 March 2006; published 22 June 2006)

Interatomic Coulombic decay (ICD) from an Auger-final dicationic state is observed in the Ar dimer. A $2p$ inner-shell vacancy created by photoionization is replaced with $3s$ and $3p$ vacancies via intra-atomic Auger decay. The Auger-final dicationic state is subject to ICD in which one of the $3p$ electrons in the same Ar atom fills the $3s$ vacancy while one of the $3p$ electrons from the neighboring Ar atom is emitted as an ICD electron. This ICD process is unambiguously identified by electron-ion-ion coincidence spectroscopy in which the kinetic energy of the ICD electron and the kinetic energy release between Ar^+ and Ar^{2+} are measured in coincidence.

DOI: [10.1103/PhysRevLett.96.243402](https://doi.org/10.1103/PhysRevLett.96.243402)

PACS numbers: 36.40.Mr, 33.60.Fy, 34.30.+h, 82.33.Fg

When an electron from an inner-shell orbital localized at a particular atomic site in the system is ionized, the inner-shell ionized atom undergoes Auger decay in which the inner-shell vacancy is filled by one of the valence electrons and another valence electron is ejected (the Auger electron [1]). Nearly a decade ago, Cederbaum *et al.* [2] proposed a new mechanism of electronic decay where the environment plays a role. An isolated atom or molecule with an *inner-valence* vacancy is generally not subject to Auger decay but may be subject to interatomic or intermolecular Coulombic decay (ICD) if it is in close proximity to other species. The *interatomic* nature of ICD is in contrast to the usual Auger decay which is basically *intra-atomic*. In ICD, an atom with an inner-valence vacancy can transfer its energy to a neighboring species which subsequently releases its energy by emitting an electron from its outervalence orbital [3]. As illustrated below, the ICD process is often interpreted as a transfer of a virtual photon between the two atoms or cluster units, which rests on the neglect of the orbital overlap between them. Averbukh *et al.*, however, showed that even in loosely bound van der Waals clusters the orbital overlap is a crucial factor [4]. Furthermore, Santra *et al.* demonstrated that ICD emerges in clusters following intra-atomic Auger decay, using extensive *ab initio* calculations for the neon dimer as a prototype sample [5].

Stimulated by the theoretical work of Cederbaum and co-workers [2,3], Marburger *et al.* [6] studied experimentally the ICD process in $2s$ ionized Ne clusters. Later, Jahnke *et al.* [7] reported very convincing, clear experimental evidence for ICD in $2s$ ionized Ne dimers by identifying the process unambiguously using electron-ion-ion coincidence spectroscopy in which the kinetic energy of the ICD electron and the total kinetic energy release (KER) between the two Ne^+ ions were measured in

coincidence. To our knowledge, there has been no report of an experimental study of the ICD process following Auger decay, although it is relevant to numerous physical, chemical, and biological phenomena involving inner-shell vacancies in atoms and molecules in various environments. In the present Letter, we report on such a study.

The ICD process that follows Auger decay predicted by Santra *et al.* [5] is as follows. After creation of a $1s$ vacancy, $KL_1L_{2,3}$ Auger emission takes place and the $1s$ vacancy is replaced by a $2s$ and a $2p$ vacancy in a single neon atom. The atomic triple ionization threshold lies higher than the $\text{Ne}^{2+} 2s^{-1}2p^{-1}$ Auger final states. However, ICD emerges in the Ne dimer because the triple ionization threshold of the dimer lies below these Auger final states: in ICD, one of the $2p$ electrons falls into the $2s$ vacancy in the same Ne atom, emitting a virtual photon, and the neighboring Ne atom absorbs this virtual photon and emits one of the $2p$ electrons as an ICD electron. In our experiment, we employ the Ar dimer, which shows analogous processes. The schematic sequence is illustrated in Fig. 1. In the first step, after creation of a $2p$ vacancy via photoionization, $L_{2,3}M_1M_{2,3}$ Auger emission replaces one $2p$ vacancy with one $3s$ vacancy and one $3p$ vacancy within the same Ar atom [Fig. 1(a)]. The Ar_2^{2+} dimer ion then undergoes ICD, with the $3s$ vacancy being filled by a $3p$ electron from the same Ar atom, emitting a virtual photon, and the neighboring Ar atom absorbing the virtual photon and emitting one of the $3p$ electrons as an ICD electron [Fig. 1(b)]. Finally, fragmentation into Ar^+ and Ar^{2+} occurs by Coulomb explosion [Fig. 1(c)]. For atomic Ar, however, the single-configuration picture described above does not hold in a strict sense since the dicationic states which have dominant $3s^{-1}3p^{-1}$ configuration in atomic Ar^{2+} are energetically forbidden to undergo ICD in the Ar_2^{2+} dimer. In our experiment, we thus focus on the

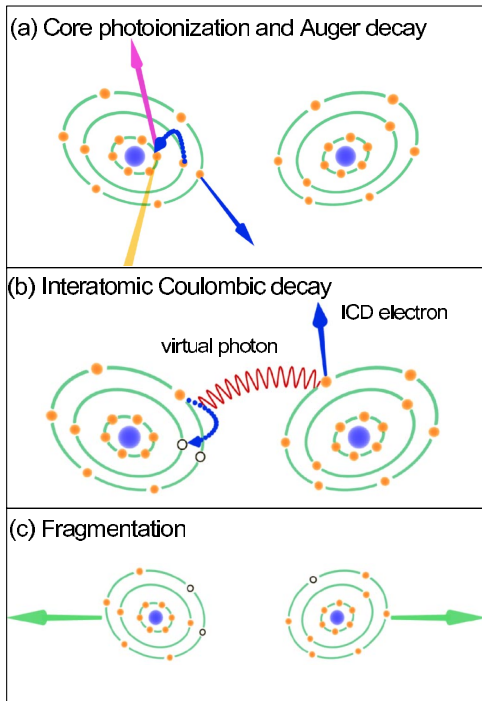


FIG. 1 (color online). Sequence of events observed in the Ar dimer. (a) Photoionization creates a $2p$ vacancy in one of the atoms. The $2p$ vacancy is filled by one of the $3s$ electrons and a $3p$ electron is emitted from the same atom (Auger decay). (b) Interatomic Coulombic decay takes place, in which the $3s$ vacancy is filled by one of the $3p$ electrons from the same atom and the excess energy is transferred to the neighboring atom which in turn emits one of its $3p$ electrons. (c) Fragmentation due to Coulomb explosion takes place. The Ar^{2+} and Ar^+ fragment ions along with the ICD electron emitted in (b) are detected in coincidence.

configuration-mixed state in which $3p^{-3}3d$ and $3s^{-1}3p^{-1}$ configurations are strongly mixed in atomic Ar^{2+} . This state is not subject to autoionization in atomic Ar^{2+} but can be subject to ICD in the Ar_2^{2+} dimer.

Our experimental approach is similar to that of Jahnke *et al.* [7]. We employ electron-ion-ion coincidence spectroscopy in which the kinetic energy of the ICD electron and the KER between Ar^+ and Ar^{2+} are measured in coincidence. The energy difference between the Auger final states (i.e., the initial state of ICD) and the two fragment atomic ions (i.e., the final state) is equal to the sum of kinetic energy of the ICD electron and the KER in the fragmentation. Thus our coincidence measurement allows us to unambiguously identify the ICD process following Auger decay.

The experiments were carried out on the c branch of the soft x-ray photochemistry beam line 27SU [8] at SPring-8. The storage ring was operated in the 35 single-bunches +6/42 filling mode, which provides a single-bunch separation of 114.0 ns. Argon dimers were produced by expanding argon gas at a stagnation pressure of 2 bar cooled

to a temperature of about 170 K through a pinhole of $30\ \mu\text{m}$ diameter and 0.25 mm thickness. The molecular beam was directed vertically and the dimer fraction in the molecular beam was determined to be at least 2%. The photon beam was focused to a size of less than 0.2 mm in height and 0.5 mm in width at the point of crossing with the molecular beam. The coincidence measurements described below were performed with the E vector orientated vertically, at a photon energy of 257.05 eV, i.e., 8.4 and 6.3 eV above the atomic Ar $2p^{-1}2P_{3/2}$ and $2p^{-1}2P_{1/2}$ ionization thresholds [9]. The photon bandwidth was ~ 30 meV.

Our electron-ion-ion coincidence momentum imaging is based on recording the electron and ion times of flight (TOFs) with multihit two-dimensional position-sensitive detectors. Knowledge of position and arrival time on the particle detectors, (x , y , and t), allows us to extract information about the linear momentum (p_x , p_y , and p_z) for each particle. The two TOF spectrometers are placed face to face, and the TOF spectrometer axis is horizontal and perpendicular to both the photon beam and the molecular beam. The apparatus employed has been newly constructed [10], based on that used for previous measurements [11–14]. The lengths of the acceleration region and the drift region of the electron spectrometer are 33.7 and 67.4 mm. For the ion spectrometer, the length of the acceleration region is 16.5 mm and no drift region is provided. The TOF spectrometer for the electron is equipped with a hexagonal multihit position-sensitive delay line detector of effective diameter of 120 mm, while that for the ion is of effective diameter 80 mm [15]. The static extraction field was set to ~ 1.53 V/mm, while a uniform magnetic field of 4.5 G was superimposed to the spectrometer by a set of Helmholtz coils outside the vacuum chamber. Under these conditions, all the electrons up to ~ 12 eV in kinetic energy and all the Ar^+ and Ar^{2+} ions up to ~ 14 eV kinetic energy, both ejected in 4π sr, were accelerated onto the MCP detectors. The TOFs of the electrons and ions were recorded with respect to the bunch marker of the synchrotron radiation source using ultrafast multihit time-to-digital converters (TDCs, c027, Hoshin Electronics Co. Ltd.) [16]. These TDCs have a timing resolution of about 120 ps, a multihit capability of up to 6 events, and a time span of 40 μs . Appropriate gates select only those electron signals synchronized with the single bunches, and we record only events in which at least one ion and one electron are detected in coincidence.

Figure 2 shows an Ar dimer ion-ion coincidence spectrum. The x and y coordinates correspond to the TOFs of the first and the second ions of the coincidence pair. Ar^{2+} and Ar^+ ions with zero momentum are located at TOFs of 3.53 and 5.09 μs , illustrated by dashed (Ar^{2+}) and dotted (Ar^+) lines in the figure. One can see clearly the lines corresponding to fragmentation into $\text{Ar}^+ - \text{Ar}^+$ and $\text{Ar}^{2+} - \text{Ar}^+$. The experimental count rate for fragmentation into $\text{Ar}^{2+} - \text{Ar}^+$ is about 30% of that into $\text{Ar}^+ - \text{Ar}^+$.

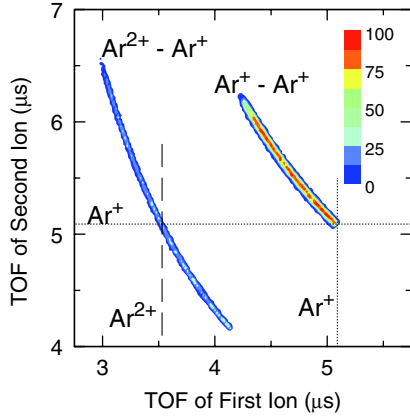


FIG. 2 (color online). Ar dimer ion-ion coincidence TOF spectrum. The dashed line shows the time-of-flight for zero-momentum Ar^{2+} ions, the dotted line for zero-momentum Ar^+ ions.

This ratio is much larger than the ratio of the double Auger process in the Auger decay in atomic Ar, which is ~ 0.1 [17]. The high production rate of $\text{Ar}^{2+} - \text{Ar}^+$ suggests that, besides the atomic double Auger process, there is an additional process that emits three electrons in total from the Ar dimer.

Our coincidence measurement for one electron and two ions provides the electron kinetic energy together with the KER between the two ions for each event. The relationship of the electron energy and the KER in the fragmentation into $\text{Ar}^{2+} - \text{Ar}^+$ is shown in Fig. 3. Figure 3(b) shows the electron energy distribution in coincidence with the fragmentation into $\text{Ar}^{2+} - \text{Ar}^+$. The two peaks located at 6.5 and 8.7 eV correspond to photoelectrons from the Ar $2p_{1/2}$ and $2p_{3/2}$ inner shells. These energies coincide with the atomic energies within an experimental uncertainty of < 0.2 eV, as previously reported [14]. The peak at ~ 2.1 eV corresponds to the ICD electrons, as we will discuss below. Figure 3(c) shows the distribution of the

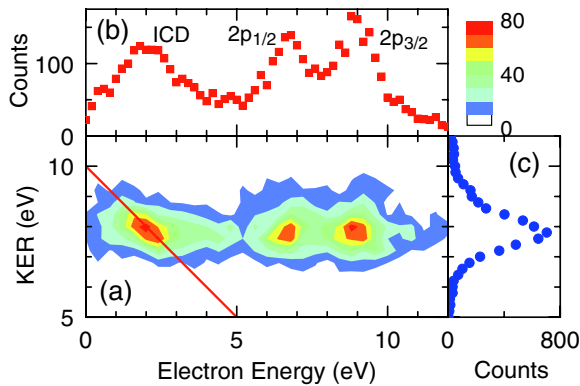


FIG. 3 (color online). (a) Relationship between the electron energy and the total kinetic energy release (KER) of the Ar_2 fragmentation. (b) Electron energy distribution of the electron ejected from Ar dimers. (c) The KER of the Ar_2 fragmentation.

KER between Ar^{2+} and Ar^+ from the Ar dimer. The mean energy is 7.8 eV, which is close to the energy of 7.7 eV calculated from the bond length of the neutral Ar dimer 3.76 \AA [18]. The KER measured in coincidence with the ICD electron is the same as that with the Ar $2p$ photoelectrons, because the ICD is the main process that leads to the fragmentation into $\text{Ar}^{2+} - \text{Ar}^+$. Figure 3(a) shows the correlation between the electron energy and the KER. There are three “islands”. The two islands in the right-hand side are attributed to photoelectrons as described above. The island on the left hand side tilts with a slope of -1 , suggesting that the sum of the electron energy and the KER is constant. The location of this island is independent of the photon energy, whereas the photoelectron islands move proportionally. Thus we can identify this island as corresponding to the ICD process following the atomic Auger decay. The total energy between the ICD electron and KER is 9.9 eV. Analogous to the Ne cluster case, although the time scale for the ICD in the Ar dimer is expected to be longer than a few fs, this slow ICD rate does not affect the dissociation dynamics, because the nuclear motion is slower than this time scale in the dimer [3,5,6,19].

We now discuss the assignment of the levels involved in the observed ICD process. The relevant Auger final states of atomic Ar [20] are listed in Table I. In the single-configuration approximation the two-vacancy Auger final states of atomic Ar^{2+} are $3p^{-2}$, $3s^{-1}3p^{-1}$, and $3s^{-2}$. In the case of atomic Ar^{2+} , however, the single-configuration approximation completely breaks down. The two configurations $3s^{-1}3p^{-1}$ and $3p^{-3}3d$ are completely mixed and contribute equally to both in dicationic states at 61.23 and 70.64 eV. As a result, the Ar atomic Auger transition to the state at 70.64 eV designated as $3p^{-3}3d^1P$ occurs with significant intensity. The Auger lines of atomic Ar at 180.06 and 177.91 eV assigned to $L_{2,3}M_1M_1$ by Siegbahn *et al.* [21] are in fact the transitions to this configuration-mixed state at 70.64 eV. The triple ionization threshold of

TABLE I. Ionization potentials of atomic Ar and dimer Ar_2 relevant to the ICD [20].

Charge	Designation	Energy (eV)
Ar^+	$3p^{-1}2P_{3/2}$	15.75
Ar^{2+}	$3p^{-2}3P_2$	43.37
Ar^{2+}	$3p^{-2}1D_2$	45.11
Ar^{2+}	$3p^{-2}1S_0$	47.49
Ar^{2+}	$3s^{-1}3p^{-1}3P$ (76%) (+ $3p^{-3}3d^3P$ (17%))	57.48
Ar^{2+}	$3s^{-1}3p^{-1}1P$ (43%) (+ $3p^{-3}3d^1P$ (50%))	61.23
Ar^{2+}	$3p^{-3}3d^1P$ (48%) (+ $3s^{-1}3p^{-1}1P$ (37%))	70.64
Ar^{2+}	$3s^{-2}1S$	74.34
Ar^{3+}	$3p^{-3}4S_{3/2}$	84.27
Ar_2^{3+}	$3p^{-2}3P + 3p^{-1}2P + \text{KER}$ (7.8 eV)	66.9
Ar_2^{3+}	$3p^{-2}1D_2 + 3p^{-1}2P + \text{KER}$ (7.8 eV)	68.7
Ar_2^{3+}	$3p^{-2}3S_0 + 3p^{-1}2P + \text{KER}$ (7.8 eV)	71.0

atomic Ar (84.27 eV) is above any Auger final states listed in Table I and thus these states are not subject to autoionization in an isolated Ar atom. However, the triple ionization threshold for the Ar₂ dimer is significantly lower, as shown in the last three lines of Table I, where the triple ionization potentials are estimated as the sum of the energies of the Ar²⁺ and Ar⁺ states and the KER (7.8 eV). The state at 61.23 eV designated as 3s⁻¹3p⁻¹1P is not subject to ICD. However, the state at 70.64 eV designated as 3p⁻³3d¹1P is subject to ICD. It is worth noting that, though this state is populated via atomic Auger decay via the mixed configuration component 3s⁻¹3p⁻¹, as noted above, both 3p⁻³3d and 3s⁻¹3p⁻¹ configurations contribute to ICD: the 3d electron (one of the 3p electrons) in the 3p⁻³3d (3s⁻¹3p⁻¹) configuration jumps to the 3p (3s) orbital via virtual photon emission, while the other Ar atom virtually absorbs the photon and emits one of the 3p electrons as an ICD electron. The final states of ICD (virtual photon exchange) can be Ar²⁺3p⁻²3P + Ar⁺3p⁻¹2P and Ar²⁺3p⁻²1D + Ar⁺3p⁻¹2P (see Table I). The estimated kinetic energy of the ICD electron is 3.7 and 1.9 eV for former and latter final states, and the observed ICD peak at 2.1 eV coincides well with the expected value of 1.9 eV. The ICD final state is thus assigned mostly to Ar²⁺3p⁻²1D + Ar⁺3p⁻¹2P. ICD to Ar²⁺3p⁻²3P + Ar⁺3p⁻¹2P is also likely to be observed on the higher-energy side but limited experimental resolution prevented us from separating this component.

Genotoxic damage by high-energy ionizing radiation (α , β , x , and γ rays), including the breaking of DNA strands in living cells, is not caused by direct ionization but is induced by the secondary particles produced by the primary ionizing radiation. Low-energy secondary electrons are the most abundant of these secondary particles, and Boudaïffa *et al.* [22] have found that low-energy (1 to 20 eV) electrons can break DNA strands. Later, Hanel *et al.* [23] demonstrated that the uracil molecule, one of the base units of RNA, is efficiently fragmented by electrons with energies <1 eV, i.e., below the threshold for electronic excitations. The ICD can undergo in biological molecules in the biological environment, following Auger decay as well as inner-valence ionization caused by incident radiation as well as by the secondary process. Generally, the kinetic energy of the ICD electron is much lower than that of the atomic Auger electron. Thus, one can expect that at least a relevant portion of the secondary low-energy electrons generated by high-energy ionizing radiation are generated via ICD.

In conclusion, we have unambiguously identified the ICD process from the Auger final state in the Ar dimer by simultaneously determining the kinetic energy of the ICD electron and the KER between Ar⁺ and Ar²⁺ using an electron-ion-ion coincidence technique. We emphasize that ICD following atomic Auger decay is a very general decay channel leading to the emission of low-energy elec-

trons following inner-shell ionization and is relevant to numerous physical, chemical, and biological phenomena involving inner-shell vacancies in clusters and other forms of spatially extended atomic and molecular matter, such as biological molecules in biological environment.

The experiments were performed at SPring-8 with the approval of the program review committee (No. 2005B0408 and No. 2005B0497-NSb-np). The work was partly supported by Grants-in-Aid for Scientific Researches from the Japan Society for Promotion of Science and by the Budget for Nuclear Research from Ministry of Education, Culture, Sports, Science and Technology, based on screening and counseling by the Atomic Energy Commission. We are grateful to J.R. Harries for a critical reading of the manuscript.

*Electronic address: norio.saito@aist.go.jp

†Electronic address: ueda@tagen.tohoku.ac.jp

- [1] M. Thompson *et al.*, *Auger Electron Spectroscopy* (Wiley, New York, 1985).
- [2] L. S. Cederbaum, J. Zobeley, and F. Tarantelli, *Phys. Rev. Lett.* **79**, 4778 (1997).
- [3] R. Santra, J. Zobeley, L. S. Cederbaum, and N. Moiseyev, *Phys. Rev. Lett.* **85**, 4490 (2000).
- [4] V. Averbukh, I. B. Müller, and L. S. Cederbaum, *Phys. Rev. Lett.* **93**, 263002 (2004).
- [5] R. Santra and L. S. Cederbaum, *Phys. Rev. Lett.* **90**, 153401 (2003); **94**, 199901(E) (2005).
- [6] S. Marburger, O. Kugeler, U. Hergenbahn, and T. Möller, *Phys. Rev. Lett.* **90**, 203401 (2003).
- [7] T. Jahnke, *et al.*, *Phys. Rev. Lett.* **93**, 163401 (2004).
- [8] H. Ohashi *et al.*, *Nucl. Instrum. Methods Phys. Res., Sect. A* **467–468**, 529 (2001); **467–468**, 533 (2001).
- [9] G. C. King, M. Tronc, F. H. Read, and R. C. Bradford, *J. Phys. B* **10**, 2479 (1977).
- [10] Y. Morishita *et al.*, *Radiat. Phys. Chem.* (to be published).
- [11] Y. Muramatsu *et al.*, *Phys. Rev. Lett.* **88**, 133002 (2002).
- [12] A. De Fanis *et al.*, *Phys. Rev. Lett.* **89**, 023006 (2002).
- [13] N. Saito *et al.*, *J. Phys. B* **36**, L25 (2003).
- [14] A. De Fanis *et al.*, *J. Phys. B* **37**, L235 (2004).
- [15] see <http://www.roentdek.com> for details on the detectors.
- [16] Y. Morishita *et al.*, *J. Electron Spectrosc. Relat. Phenom.* **144–147**, 255 (2005).
- [17] N. Saito and I. H. Suzuki, *J. Electron Spectrosc. Relat. Phenom.* **88–91**, 65 (1998); *Phys. Scr.* **49**, 80 (1994).
- [18] E. A. Colbourn and A. E. Douglas, *J. Chem. Phys.* **65**, 1741 (1976).
- [19] G. Öhrwall *et al.*, *Phys. Rev. Lett.* **93**, 173401 (2004).
- [20] http://physics.nist.gov/PhysRefData/ASD/levels_form.html
- [21] K. Siegbahn *et al.*, *ESCA Applied to Free Molecules* (North-Holland, Amsterdam, 1969).
- [22] B. Boudaïffa, P. Cloutier, D. Hunting, M. A. Huels, and L. Sanche, *Science* **287**, 1658 (2000).
- [23] G. Hanel *et al.*, *Phys. Rev. Lett.*, **90**, 188104 (2003).